J Mater Sci (2009) 44:6416–6422
DOI 10.1007/s10853-009-3885-x

Effect of interstitial lithium atom on crystal and electronic structure of silicon oxynitride

Bin Liu · Jingyang Wang · Fangzhi Li · Hongqiang Nian · Yanchun Zhou

Received: 1 April 2009 / Accepted: 11 September 2009 / Published online: 25 September 2009

Abstract Plane-wave pseudopotential total energy method was used to calculate the effects of impurity Li atom on crystal structure, electronic and dielectric properties of Si_2N_2O. It is proved that Li atom prefers to occupy interstitial site than to substitute the Si atomic site. In addition, the presence of interstitial Li atom leads to relaxation of internal coordinates of Si, N, and O atoms, and bring out a different X-ray diffraction (XRD) pattern compared with that of a pure Si_2N_2O. The result is helpful to understand the diversity of experimental XRD data for Si_2N_2O sintered with and without Li_2O additive. The theoretical polycrystalline dielectric constant of Li-doped Si_2N_2O is larger than that of a pure one, which can be attributed to a reduction of band gap. The mechanism is that interstitial Li atom provides extra electronic states at the bottom of conductive band.

Introduction

Compounds in the Si–O–N system exhibit excellent thermal, chemical, and mechanical stability, as well as high diffusion barrier and good dielectric properties [1]. Stoichiometric silicon oxynitride (Si_2N_2O) is a refractory material with all the aforementioned and desirable properties, and also has enhanced performance compared with SiO_2- and Si_3N_4-based devices [2–5]. Synthesis of Si_2N_2O has been the recent focus of intense researches because of its potential applications for high-temperature engineering component and has been achieved by sintering equimolar SiO_2 and Si_3N_4 powders with additives. In the past years, some theoretical and experimental studies have been done to understand the influence of defects on both the microstructure and property for bulk material and inter-granular films of Si_2N_2O with the aim to control their appearance and concentration [6–8].

Recently, a new synthesizing method to prepare Si_2N_2O with Li_2O additive is reported by Tong et al. [9]. Compared with using other metal oxide sintering additives, the sintering temperature of using Li_2O additive is greatly lowered and the firing time is shortened to get pure and dense Si_2N_2O. Furthermore, Si_2N_2O synthesized in this method still keeps good mechanical and dielectric performances. However, the effect of Li on the structure and properties of Si_2N_2O is not well understood and need to be clarified because of the following reasons: Li easily enters Si_2N_2O forming point defects due to its small size. Unfortunately, it is hard to investigate the mechanism of small amount of Li being in Si_2N_2O lattice. On the other hand, it is known that crystal structure, electronic structure, and electrical/optical properties of insulating ceramics are affected and even deteriorated due to the existence of intrinsic and heterogeneous defects. Influence of doped Li atoms on the optical and electrical properties of some ceramics, such as ZnO, V_2O_5, and $Li_3Fe_2(PO4)_3$ [10–12], has been widely studied. For the present case, it is observed that the polycrystalline dielectric constant of Si_2N_2O enhanced with the increase of

B. Liu · J. Wang · F. Li · H. Nian · Y. Zhou
Shenyang National Laboratory for Materials Science, Institute of Metal Research, Chinese Academy of Sciences, 110016 Shenyang, China

B. Liu · F. Li · H. Nian
Graduate School of Chinese Academy of Sciences, 100039 Beijing, China

J. Wang (✉)
High-performance Ceramic Division, Institute of Metal Research, Chinese Academy of Sciences, 110016 Shenyang, China
e-mail: jywang@imr.ac.cn

residual Li content [9]. Thus, investigation of lithium-doped Si_2N_2O is of technological significance to understand the electronic structure and electrical/optical properties of experimentally synthesized compound. In addition, a large discrepancy appears between XRD pattern of Si_2N_2O prepared with Li_2O additive and that prepared by other methods [9, 13]. Both the intensity and the height of some peaks conflict within each other in different XRD patterns [9, 13]. Until now, a satisfied explanation was not provided about this experimental phenomenon.

Characterization of point defects in material is typically quite hard without the help of theoretical calculation. Density functional theory (DFT) has been successfully used to study the defective structure of polymorphous TiO_2 [14, 15] and pyrochlore type rare earth oxides ($Re_2Zr_2O_7$, Re = rare earth) [16, 17]. Thus, a first-principle investigation of Li-doped Si_2N_2O is necessary, which will serve as a firm basis to understand defect-related phenomena and provide a new sight to recognize these phenomena in electron scale. Ching [18] and Xu and Ching [19] have systematically investigated the electronic structure and dielectric constant of the compounds in Y–Si–O–N phase equilibrium diagram including Si_2N_2O by DFT method. Liu et al. [8] have studied the native point defect and nonstoichiometry in Si_2N_2O combining DFT and force-field method, in which the oxygen/nitrogen antisites dominate the native defect and accommodate the deviations from stoichiometry. However, no paper ever reported effects of impurity atoms on the properties of Si_2N_2O. In the present work, we employ DFT calculations to study the changes of crystal structure and electronic structure originated from Li doping. Then, we further explain the diversity of experimental XRD data for Si_2N_2O sintered with and without Li_2O additive. Furthermore, the enhancement of polycrystalline dielectric constant of Si_2N_2O after Li doping is also discussed based on an analysis of electronic structure. The present theoretical investigation provides a comprehensive insight into the effect of impurity Li atom on structure and properties of Si_2N_2O.

Calculation method

Theoretical investigations were accomplished by using the CASTEP code [20], employing the Vanderbilt-type ultrasoft pseudopotential [21] and local density approximations [22] (LDA). The plane wave energy cutoff and the Brillouin zone sampling were fixed to 450 eV and $3 \times 2 \times 3$ special k-point meshes, respectively [23]. Lattice parameters, including lattice constants and internal atomic coordinates, were modified independently to minimize the free enthalpy, interatomic forces, and unit-cell stresses. The Brodyden–Fletcher–Goldfarb–Shanno (BFGS) minimization scheme [24] was used in geometry optimization. The tolerances for geometry optimization were: difference on total energy within 5×10^{-6} eV/atom, maximum ionic Hellmann–Feynman force within 0.01 eV/Å, maximum ionic displacement within 5×10^{-4} Å, and maximum stress within 0.02 GPa. These parameters were sufficient in leading to well-converged total energy and geometrical configurations. Increasing the plane-wave cutoff energy to 550 eV and the k-point mesh to $4 \times 3 \times 4$ changed the total energy less than 0.009 eV/atom. Furthermore, the present first-principle calculation scheme was reliable for predicting crystal structure, elastic stiffness, and inter-atomic force constants of ternary carbides [25–27] and complex oxides such as $LaPO_4$ monazite [28], Si_2N_2O [8] and $La_2Zr_2O_7$ pyrochlore [29].

The diagonal components of the dielectric function (ε) can be expressed as $\varepsilon = \varepsilon_1 + i\varepsilon_2$, in which [30]

$$\varepsilon_1 = 1 + \frac{2}{\pi} p \int_0^\infty \frac{v\varepsilon_2(v)}{v^2 - \omega^2} \mathrm{d}v \tag{1a}$$

$$\varepsilon_2 = \frac{\hbar e^2}{3\pi m^2 \omega^2} \times \sum_{l,j} \int d^3k |M_l(k)|^2 \delta(E_l - E_j - \hbar\omega) \tag{1b}$$

Here p is the moment operator, ω is the angular frequency of light, the subscripts l and j denote the conduction and the valence bands, respectively, e and m represent the charge and the mass of electron, $M_l(k)$ is the momentum matrix element with wave vector k.

The point defect structure was represented by a $1 \times 2 \times 2$ super-cell containing 16 Si_2N_2O formulas (80 atoms in number) and 1 Li atom located at the interstitial site or substituted 1 Si atom. In defect calculations, lattice parameters and atomic positions were fully relaxed without any symmetry constraints. Formation energy $E_{\text{formation}}^{\text{defect}}$ of point defect in Si_2N_2O was calculated by:

$$E_{\text{formation}}^{\text{defect}} = E_{\text{d}} - E_p \pm \mu_i \tag{2}$$

where E_{d} is the total energy for a defective lattice, E_p the energy for a defect-free super-cell, and μ_i the chemical potential in pure solid of each species, together with "+" for vacancy and "−" for interstitial atom. This equation represents the equilibrium between Si_2N_2O and pure solid of the i component.

The calculated structure discrepancy of the Li-doped Si_2N_2O and the pure one was characterized by X-ray diffraction simulations. An X-ray diffractometer with Cu Kα radiation, including both $K\alpha_1$ and $K\alpha_2$ ($\lambda_1 = 1.540562$ Å, $\lambda_2 = 1.54439$ Å, and $I_2/I_1 = 0.5$), was used to obtain the Bragg reflection from the structure model of Si_2N_2O. At the same time, the Bragg–Brentano correction is applied to the data. Because there was no monochromator, the

polarization correction combined with Lorentz factor, L_p, was defined as

$$L_p = \frac{p + (1-p)\cdot\cos^2 2\theta}{\sin\theta\cos 2\theta} \quad (3)$$

where $p = 0.5$ was the polarization fraction, and θ was the diffraction angle. The grain size used here is 3 μm which is consistent with the experimental one [9].

Results and discussion

Crystal structure of Si_2N_2O

Before investigation of the Li-doped Si_2N_2O, we calculated the structural configuration of the pure one that possessed the local minimum total energy at first. For Si_2N_2O, any of the three types of atoms (Si, N, O) has only one crystallographic equivalent site, as a consequence of the adopted $Cmc2_1$ symmetry [31]. And the N and Si atoms are, respectively, in three- and fourfold coordination as those in Si_3N_4 [32], while the oxygen atom locates at a mirror plane and bridge Si–N slabs through Si–O–Si bonds as shown in Fig. 1. Optimized lattice constants are listed in Table 1, together with values obtained by other first-principle calculation [18, 19] and experiment [33] for comparison. The computed lattice constant deviates from previously reported data within 1%. Density, bond lengths, and the Si–O–Si bond angle are also listed in Table 1 to further validate the calculated crystal structure. The present results are in good agreement with the experimental values with a maximum deviation of 3.8% on Si–O–Si angle, which further confirms the reliability of the calculated results.

Defect structure of the Li-doped Si_2N_2O

For an impurity lithium atom in Si_2N_2O, two possible sites were considered: occupation of interstitial site and substitution of Si atomic site. For the case of Li substitution of Si atom, it is easy to achieve by Li atom taking any Si site because there is only one Si crystallographic equivalent site in Si_2N_2O. However, for the interstitial case, we need to search the preferred interstitial site at first. Due to the complex crystal structure and low symmetry of Si_2N_2O, one possible way to search the preferred interstitial site is to map out the potential energy surface as a function of three independent coordinates of interstitial Li atom. The details for determining interstitial site are as follows: firstly, the possible interstitial site should locate at the large open space between adjacent Si–N slabs and could not occupy extremely small open space inside the Si–N slab. Furthermore, the mirror plane of oxygen atoms divides the space between adjacent Si–N slabs into two equal parts

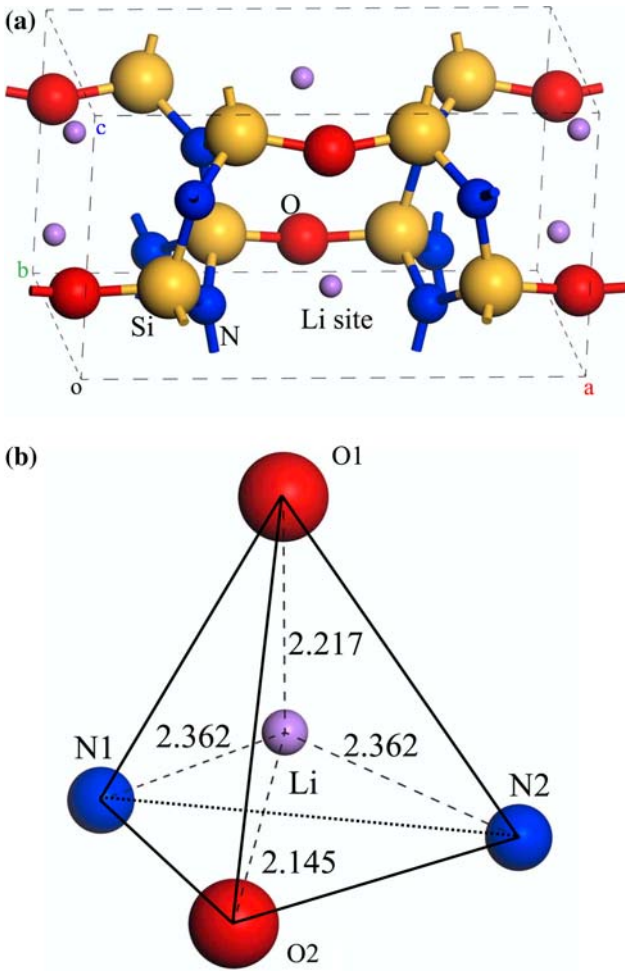

Fig. 1 **a** The optimized crystal structure of Si_2N_2O and the crystallographic inequivalent atoms are signed. Interstitial position in Si_2N_2O is also shown in (**a**) and the tetrahedron around it is illustrated in (**b**)

because of the $Cmc2_1$ symmetry of crystal structure. Therefore, only half open space between adjacent Si–N slabs were investigated to search preferred interstitial site. The present consideration also excluded those interstitial sites when a distance between Li atom and other atoms was shorter than 1 Å.

We tested two internal coordinates along the (100) direction for Li atom: $x = 0.35$ (the interstitial site located between the Si–N slabs and oxygen plane) and $x = 0.5$ (the interstitial site in oxygen plane), and change in the values of other internal coordinates y and z from 0 to 1 with a step of 0.25 increment. During searching the possible interstitial site, 19 initial geometry with different Li sites were built. Thereafter, 19 geometry optimizations were conducted to fully relax lattice constants and internal atomic coordinates of starting structure in order to minimize total energy. For all the cases, the optimized crystal structures converge to the same equilibrium configuration whatever the starting structure is. Therefore, the preferred interstitial site is determined

Table 1 Calculated lattice parameters and dielectric constants for both undoped and Li-doped Si_2N_2O. The previously reported values from both simulation and experiment are also included for comparison

	Si_2N_2O with I_{Li}	Si_2N_2O without I_{Li}		
		This work	Calc.	Expt. [33]
a (Å)	8.814	8.790	8.874 [18], 8.843 [19]	8.866
b (Å)	5.444	5.450	5.489 [18], 5.437 [19]	5.486
c (Å)	4.804	4.801	4.846 [18], 4.835 [19]	4.845
ρ (g/cm^3)	2.90	2.89	2.82 [18], 2.86 [19]	2.82
Si–N(1) (Å)	–	1.702	1.714 [19] (average)	1.701
Si–N(2) (Å)	–	1.709		1.731
Si–N(3) (Å)	–	1.703		1.711
Si–O (Å)	–	1.601	1.623 [19]	1.645
Angle (Si–O–Si) (°)	–	153.0	147.4 [19]	149.5
Dielectric constant	3.58	2.97	2.91 [18], 3.34 [19]	–

when the interstitial Li atom occupies the position (0.5, 0.1385, 0.2921). This interstitial site is surrounded by four anions (two N and two O) in a tetrahedron, as indicated in Fig. 1a, b. In addition, the preferred interstitial site locates in the oxygen plan. This result is reasonable because the open space between adjacent Si–N slabs is large enough to accommodate a foreign impurity atom [34].

To model geometric configuration after Li doping, we used a 1 × 2 × 2 super-cell (S122) with one Li atom. The calculated formation energy of an impurity Li atom is 1.92 eV. While, the formation energy is 9.45 eV for the case of Li substituting Si atom, which is much higher than that of the interstitial case. Therefore, impurity Li atom may occupy interstitial site in Si_2N_2O. To further validate our conclusions using the current supercell, defect formation energies for interstitial and substitutional cases are also calculated in larger 2 × 2 × 2 (S222) and 1 × 3 × 3 (S133) supercells. The calculated defect formation energy of S222 and S133 is 0.066 and 0.048 eV lower than that of S122 (1.92 eV), respectively, for the interstitial case; and 0.104 and 0.095 eV lower than that of S122 (9.45 eV), respectively, for the substitutional case. Thus, the 1 × 2 × 2 supercell is large enough to exclude the self-interaction of Li atom originated from periodical boundary calculation. So, a convincible result on influence of impurity Li atom on structure and properties of the Si_2N_2O can be obtained by using the present calculation parameters.

Effect of doped Li on structure and properties of Si_2N_2O

To understand the influence of interstitial Li atom on crystal structure, change of lattice constants needs to be considered. Therefore, we calculate the elongate ratio along *i*th direction by e_i:

$$e_i = \frac{a_i' - a_i}{a_i} \times 100\% \quad (4)$$

where, *i* denote three crystallographic axial orientations: [100], [010], and [001] (namely a, b, and c directions); a_i' and a_i denote the lattice constants along *i*th direction of Si_2N_2O with and without Li atoms, respectively. So, the elongate ratio along three axes is 0.27% (e_a), −0.11% (e_b), and 0.06% (e_c). The equilibrium lattice constants of the Li-doped Si_2N_2O exhibit an interesting change compared to the pure ones: *a* expands and *c* increases slightly; while *b* shrinks on the other hand. At the same time, the density of this compound increases due to lithium atom incorporation. This fact needs to be further discussed taking the nonuniform displacements of oxygen and nitrogen atoms around interstitial lithium into account. The distances between interstitial lithium atom and first nearest neighbor atoms before and after relaxation are shown in Table 2. The lengths for Li–O1 bond in relaxed and unrelaxed lattice is 2.217 and 2.258 Å, respectively; while those of Li–O2 bond are 2.145 and 2.175 Å, respectively. At the same time, the lengths of Li–N bonds (both N1 and N2) increase from 2.310 to 2.362 Å after lattice relaxation. It can be concluded that Li and O (both O1 and O2) atoms move closer due to the strong attraction between them, while Li–N (both N1 and N2) distances become larger. Thus, we can attribute the decreasing of *b* axis (0.006 Å) to the shrinkage of Li–O1 and Li–O2 bond lengths. Moreover, the larger expansion of *a* axis originated from the elongation of two Li–N bonds and the minor change of *c* axis can be

Table 2 Calculated distances between interstitial lithium atom and its nearest atoms for both relaxed and unrelaxed cells

	Distance (Å)	
	Unrelaxed cell	Relaxed cell
Li–O1	2.258	2.217
Li–O2	2.175	2.145
Li–N1	2.310	2.362
Li–N2	2.310	2.362

attributed to the simultaneous increasing of two Li–N distances and decreasing of Li–O2 bond length. The results show that crystal structure of Si_2N_2O is disturbed by the impurity Li atom.

It was reported that a large discrepancy appears between XRD pattern of Si_2N_2O prepared with Li_2O additive [9] and that prepared by other method [13]. To clarify the origin, we show calculated XRD patterns of pure and Li-doped Si_2N_2O in Fig. 2a, b, respectively, together with the experimental data of Si_2N_2O prepared with Li_2O additive in Ref. [9]. Three diversifications need to be considered by analyzing these pictures: firstly, the (111) peak is the highest for Li-doped Si_2N_2O while it ranks the third in height for pure Si_2N_2O. Secondly, the height discrepancy between (110) peak and (200) peak becomes small in Li-doped Si_2N_2O. Thirdly, the (002) peak increases up to fourth in height in Li-doped Si_2N_2O. These features are well consistent with the experimental one [9, 13]. Table 3 lists the calculated data of reflections, 2θ, and

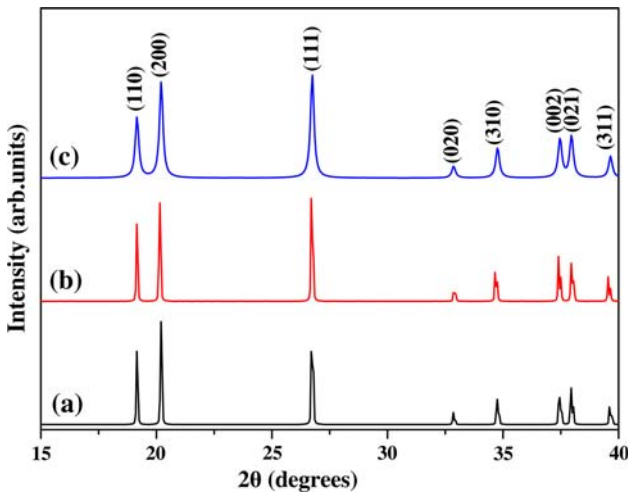

Fig. 2 XRD patterns of pure Si_2N_2O (*a*) and Li atom-doped Si_2N_2O (*b*), together with the experimental data (*c*) [9]

Table 3 Reflections, 2θ positions, and intensity data for pure and Li-doped Si_2N_2O

hkl	Pure Si_2N_2O		Si_2N_2O with I_{Li}	
	2θ (°)	I/I_0 (%)	2θ (°)	I/I_0 (%)
110	19.16	58.08	19.16	56.33
200	20.21	91.64	20.15	89.96
111	26.74	100	26.73	100
020	32.87	11.62	32.90	12.34
310	34.76	29.89	34.70	31.19
002	37.46	39.07	37.44	39.67
021	37.97	41.75	37.99	41.26
311	39.65	21.59	39.58	22.54

intensity for pure and Li-doped Si_2N_2O. The (020) peak moves to higher angle, while the (200) and (002) peaks shift to lower angle. These results well reproduce the diversification of lattice constant discussed above (*a* expands and *c* increases slightly; while *b* shrinks). Simultaneously, small shifts are observed for most peaks except for that of the (110) diffraction, and the maximum displacement 0.07° corresponds to the (311) diffraction.

To further understand the influence of interstitial Li atom on XRD pattern of Si_2N_2O, two possible mechanisms should be considered: scattering of Li atom itself and the internal relaxation of Si, N, and O atoms., Thus, two structures are built: LDS1 is modeled by locating a Li atom at interstitial site on pure Si_2N_2O ($1 \times 2 \times 2$ super-cell) without internal relaxation, which considers the effect of scattering of Li atom only. In order to evaluate the impact of internal freedom relaxation of Si, N, and O atoms, LDS2 is established by removing the interstitial Li atom after structure relaxation. Then, we simulated the XRD patterns for the two models. For simpleness, the simulated XRD patterns of LSD1 and LSD2 are not shown here because there is no obvious discrepancy between them and Fig. 2a, b, respectively. The results show that the XRD pattern of LDS2 structure is the same with that of Li-doped Si_2N_2O in simulation (Fig. 2b) and similar to experiment result (Fig. 2c) [9], while the one of LDS1 is identical to that of pure Si_2N_2O (Fig. 2a). Therefore, it can be concluded that the discrepancy of peak height of XRD patterns between Si_2N_2O with and without Li atom originates predominantly from the internal relaxation after Li doping. In other words, interstitial Li atom affects the XRD pattern of Si_2N_2O by leading internal structural relaxation. This result is helpful to understand the characteristics of experimental XRD patterns [9, 13] of Si_2N_2O containing impurity Li.

To understand the changes of electronic structure and properties, electronic density of state (DOS) of silicon oxynitride with and without interstitial Li atom are illustrated. Figure 3a shows that the total density of state (TDOS) and the projected density of state (PDOS) of pure silicon oxynitride super-cell. The lowest lying states of N and O 2p states overlap with the Si 3s states locating at around −10 to −8 eV. The states extending from −8 eV to the Fermi level originate mainly from N and O 2p orbitals with slight contributions from Si 3p states. The electronic states above the Fermi level are dominated by the Si s–p hybridization. The features are in good agreement with those reported by Ching and coworkers [18, 19]. The theoretical TDOS and PDOS calculated for Li-doped Si_2N_2O is shown in Fig. 3b. It is noted that the Fermi level of Li-doped Si_2N_2O locates at 0.83 eV above the bottom of conductive band leading to an n-type feature for Li-doped Si_2N_2O. The donor states mainly origin from Li 2s orbital that is located at the bottom of conductive band. As there

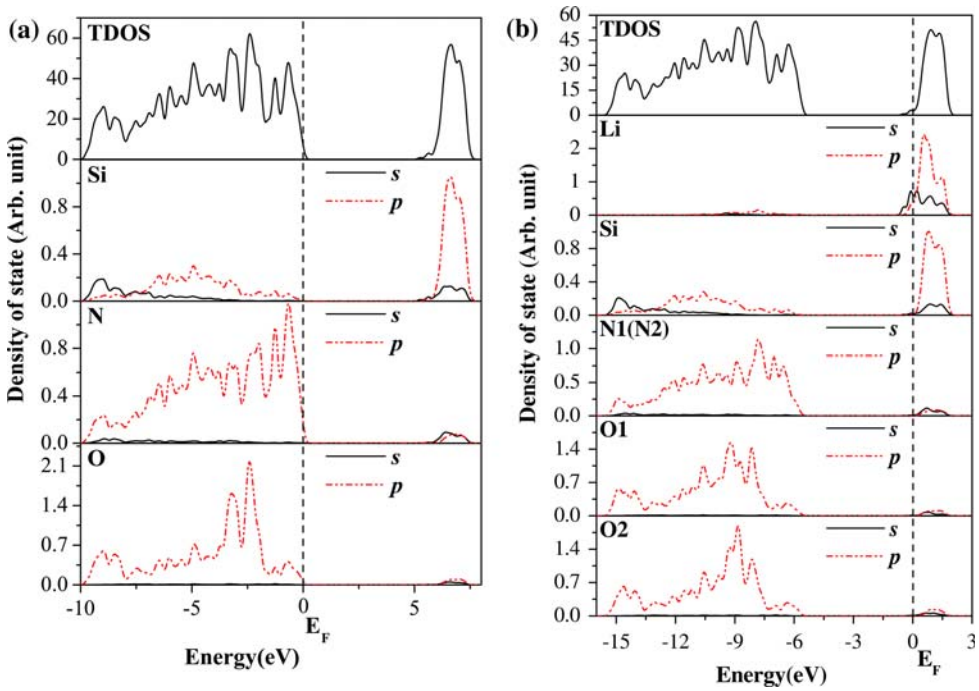

Fig. 3 TDOS (total density of states) and PDOS (projected density of states) for pure Si_2N_2O (**a**) and Li atom-doped Si_2N_2O (**b**)

are no hybridization states between Li and O atoms, the interaction is in ionic nature. Therefore, shorter Li–O distances can be attributed to the ionic attraction.

Now, we can further explain the structural change by combining the bonding and structural characteristics. As is shown above, Li and O (both O1 and O2) atoms move closer, which is the main origin of change in crystal structure. Especially, the shrinkage of Li–O1 and Li–O2 bond lengths directly leads to the constriction of *b* axis. So, it is of importance to understand the origin for the movement of O atom corresponding to interstitial Li atoms. This feature can be attributed to following reasons: firstly, ionic attraction exists between O and Li atoms. Secondly, it is known that the structure of Si_2N_2O is easily disturbed by Si–O–Si bending in the oxygen plan, which has been proven by the investigation of vibrational spectra of Si_2N_2O [35]. As a result, the O atoms move toward interstitial Li in the oxygen plan.

Because of the feasibility of using SiO_xN_y glass as a gradient index optical material [19], the optical properties of Li-doped and pure Si_2N_2O need to be known. Also the dielectric properties of crystalline Si_2N_2O are not well studied due to the lack of single-crystal samples for this compound. Figure 4 displays that the theoretical dielectric functions of polycrystalline pure and Li-doped Si_2N_2O. For pure Si_2N_2O, the real part has the highest peak at 6.9 eV, and a depression lower than zero in the 11.2–19.7 eV range, while the imaginary part has a plateau with some local peaks in 5–20 eV range. These features are in well accordance with other results [18, 19]. The real and imaginary parts of Li-doped Si_2N_2O are similar to the pure

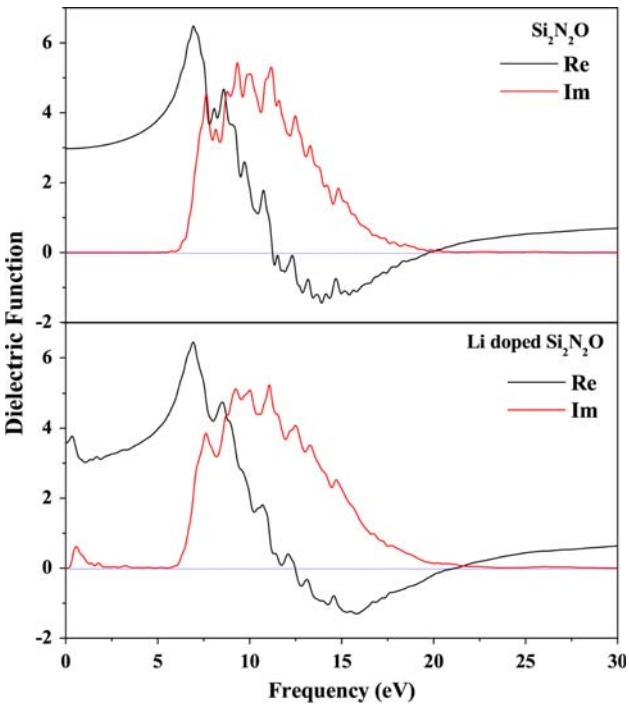

Fig. 4 Calculated real and imaginary parts of the dielectric function for pure and Li-doped Si_2N_2O

one. However, two peaks appear at 0.3 eV for real part and at 0.6 eV for imaginary part, which originate from the intraband transitions of free electronic carriers in the bottom of the conductive band. This feature has been widely observed in other compounds containing various point defects [36, 37].

The values of polycrystalline static dielectric constants of pure and Li-doped Si_2N_2O are 2.97 and 3.58 eV, respectively, as shown in Table 1. The value of the pure one is in excellent agreement with other results [18, 19]. And the polycrystalline dielectric constant of Li-doped Si_2N_2O is larger than that of pure one, which can be attributed to the reduction of band gap due to the extra states of impurity Li atom at the bottom of conductive band. This conclusion is the key to explain the experimental observation by Tong et al. [9], who found that the polycrystalline dielectric constant of Si_2N_2O enhanced with the increase of residual Li content.

Conclusion

In summary, the effect of heterogeneous impurity lithium atom on crystal structure, electronic structure, and dielectric properties of silicon oxynitride are studied by first-principle calculations. Impurity Li atom prefers to occupy the interstitial site in Si_2N_2O due to its lower defect formation energy. The crystal structure of Si_2N_2O containing impurity Li atom changes obviously, which leads to the significant diversity of XRD patterns between without and with impurity Li atoms in Si_2N_2O. Furthermore, the polycrystalline dielectric constant of Si_2N_2O containing impurity Li is larger than that of the pure one, which is attributed to the reduction of band gap.

Acknowledgements This work was supported by the National Outstanding Young Scientist Foundation for Y C Zhou, and the Natural Sciences Foundation of China under Grant Nos. 50672102 and 50772114.

References

1. Buchanan DA (1999) IBM J Res Dev 43(3):245
2. Roucka R, Tolle J, Chizmeshya AVG et al (2002) Phys Rev Lett 88:206102
3. Roucka R, Tolle J, Crozier PA et al (2001) Appl Phys Lett 79:2080
4. van Weeren R, Leone EA, Curran S et al (1994) J Am Ceram Soc 77:2699
5. Wendor P, de Ruiter R (1989) J Chem Soc Chem Commun 320
6. Devine RAB, Duraud JP, Doryhee E (2000) Structure and imperfections in amorphous and crystalline silicon dioxide. Wiely, Bognor Regis
7. Gritsenko VA, Wong H, Xu JB et al (1999) J Appl Phys 86:3234
8. Liu B, Wang JY, Li FZ et al (2009) J Phys Chem Solids 70:982
9. Tong QF, Zhou YC, Wang JY et al (2007) J Eur Ceram Soc 27:4767
10. Lu JG, Zhang YZ, Ye ZZ et al (2006) Appl Phys Lett 89:112113
11. Li ZY, Zhou CJ, Lin W et al (2007) Chin J Luminescence 28:1
12. Shirakawa J, Nakayama M, Wakihara M et al (2006) J Phys Chem B 110:17743
13. Larker R (1992) J Am Ceram Soc 75:62
14. Na-Phattalung S, Smith MF, Kim K et al (2006) Phys Rev B 73:125205
15. Cho E, Han S, Ahn HS et al (2006) Phys Rev B 73:193202
16. Panero WR, Stixrude L, Ewing RC (2004) Phys Rev B 70:054110
17. Chartier A, Meis C, Weber WJ et al (2002) Phys Rev B 65:134116
18. Ching WY (2004) J Am Ceram Soc 87:1996
19. Xu YN, Ching WY (1995) Phys Rev B 51:17379
20. Segall MD, Lindan PLD, Probert MJ et al (2002) J Phys Condens Matter 14:2717
21. Vanderbilt D (1990) Phys Rev B 41:7892
22. Ceperley DM, Alder BJ (1980) Phys Rev Lett 45:566
23. Monkhorst HJ, Pack JD (1977) Phys Rev B 16:1748
24. Pfrommer BG, Côté M, Louie SG et al (1997) J Comput Phys 131:233
25. Wang JY, Zhou YC, Liao T et al (2006) Appl Phys Lett 89:021917
26. Liu B, Wang JY, Zhang J et al (2009) Appl Phys Lett 94:181906
27. Wang JY, Zhou YC, Lin ZJ et al (2006) Phys Rev B 73:134107
28. Wang JY, Zhou YC, Lin ZJ (2005) Appl Phys Lett 87:051902
29. Liu B, Wang JY, Zhou YC et al (2007) Acta Mater 55:2949
30. Zhang HI, Callaway J (1969) Phys Rev 181:1163
31. Baraton MI, Billy M, Labbe JC et al (1988) Mater Res Bull 23:1087
32. Idrestedt I, Brosset C (1964) Acta Chim Scand 18:1879
33. Srivinasa SR, Cartz L, Jorgensen JD et al (1977) J Appl Crystallogr 10:167
34. Kroll P, Milko M (2003) Z Anorg Allg Chem 629:1737
35. Mirgorodsky AP, Baraton MI, Quintard PQ (1989) J Phys Condens Matter 1:10053
36. Guo XG, Chen XS, Lu W (2003) Solid State Commun 126:441
37. Guo ML, Zhang XD, Gu HE et al (2008) Cent Eur J Phys 6:321